Effect of Nb Addition to Ti-Bearing Super Martensitic Stainless Steel on Control of Austenite Grain Size and Strengthening

XIAOPING MA, BRIAN LANGELIER, BAPTISTE GAULT, and SUNDARESA SUBRAMANIAN

The role of Nb in normalized and tempered Ti-bearing 13Cr5Ni2Mo super martensitic stainless steel is investigated through in-depth characterization of the bimodal chemistry and size of Nb-rich precipitates/atomic clusters and Nb in solid solution. Transmission electron microscopy and atom probe tomography are used to analyze the samples and clarify precipitates/atom cluster interactions with dislocations and austenite grain boundaries. The effect of 0.1 wt pct Nb addition on the promotion of (Ti, Nb)N-Nb(C,N) composite precipitates, as well as the retention of Nb in solution after cooling to room temperature, are analyzed quantitatively. (Ti, Nb)N-Nb(C,N) composite precipitates with average diameters of approximately 24 ± 8 nm resulting from epitaxial growth of Nb(C,N) on pre-existing (Ti,Nb)N particles, with inter-particle spacing on the order of 205 ± 68 nm, are found to be associated with mean austenite grain size of 28 ± 10 μm in the sample normalized at 1323 K (1050 °C). The calculated Zener limiting austenite grain size of 38 ± 13 μm is in agreement with the experimentally observed austenite grain size distribution. 0.08 wt pct Nb is retained in the as-normalized condition, which is able to promote Nb(C, N) atomic clusters at dislocations during tempering at 873 K (600 °C) for 2 hours, and increases the yield strength by 160 MPa, which is predicted to be close to maximum increase in strengthening effect. Retention of solute Nb before tempering also leads to it preferentially combing with C and N to form Nb(C, N) atom clusters, which suppresses the occurrence of Cr- and Mo-rich carbides during tempering.

DOI: 10.1007/s11661-017-4036-7

I. INTRODUCTION

ULTRALOW carbon (<0.03 wt pct) steels with base chemical composition of 13–16 wt pct Cr, 3–5 wt pct Ni, 0.5–2.5 wt pct Mo are called super martensitic stainless steel (hereafter referred to as SMSs), and have been widely applied to critical structures and components such as turbines, marine propellers, aircraft parts, oil country tubular goods and flow lines from the wellheads to the treatment stations, transporting unprocessed fluid (crude oil or gas) at very high pressure and temperature. They exhibit an excellent combination of strength and toughness as well as corrosion resistance, but these strongly depend on its heat treatment history and chemical composition.[1–4] Further improvement in mechanical properties and localized corrosion resistance can be achieved by microalloying with Nb and Ti.[5–7] Previous research on the effect of Nb addition to Ti-bearing SMSs by the authors focused on microstructure evolution during normalizing and tempering heat treatments, and its consequence on mechanical properties and pitting corrosion resistance have been reported elsewhere.[5,6] It was found that Nb addition plays two functional roles: (i) to improve the toughness by preventing austenite grain coarsening during normalizing treatment; and (ii) to enhance the strength significantly and improve the pitting corrosion resistance after tempering. However, the mechanisms underlying these beneficial effects have not been clarified. The objective of the present paper is to address these problems through identifying the interaction of multi-level, multi-scale Nb-rich precipitates with dislocations and austenite grain boundaries in Nb microalloyed 13Cr5Ni2Mo SMSs.

II. EXPERIMENTAL PROCEDURES

The chemical compositions of the SMSs with and without Nb addition are shown in Table I. The steels were made in the form of ingots, using a 100-kg vacuum-induction furnace. The ingots were hot rolled at 1373 K (1100 °C) into plates with 12 mm thickness. Normalizing was carried out by solution treatment at 1323 K (1050 °C) for 0.5 hours for homogenization, followed by air cooling to room temperature. Subsequent tempering was performed at 873 K (600 °C) for

XIAOPING MA, BRIAN LANGELIER, and SUNDARESA SUBRAMANIAN are with the Department of Materials Science and Engineering, McMaster University, Hamilton L9H 4L7, Canada. Contact e-mail: maxpneu@hotmail.com BAPTISTE GAULT is with the Max-Planck-Institut für Eisenforschung GmbH, Department of Microstructure Physics and Alloy Design, Max-Planck-Straße 1, 40237 Düsseldorf, Germany

Manuscript submitted November 14, 2016.
Article published online March 2, 2017

2 hours followed by oil quenching (to simulate industrial processing) to room temperature.

The precipitates in the normalized and tempered samples were investigated using carbon extraction replica by a Philips CM12 transmission electron microscope (TEM), with a high-resolution FEI Titan scanning transmission electron microscope (STEM). Energy dispersive spectrometry (EDS) and electron energy loss spectrometry (EELS) in STEM were used for analysis of precipitate chemical composition. Electron backscatter diffraction (EBSD) equipped in JEOL JSM-7000F Scanning electron microscope (SEM) was performed on as-normalized samples tilted for 70 deg using high tension of 20 KV, working distance of 18 mm and step size of 0.5 μm.

Atom probe tomography (APT) was performed using a Cameca local electrode atom probe (LEAP) 4000X HR. Specimens were prepared by a standard 2-stage electro-polishing method.[8] APT experiments were performed at a base temperature of 43 K to 54 K (−230 °C to −219 °C) in laser pulse mode (λ = 355 nm), with a pulse energy of 60 pJ, a pulse rate of 250 kHz, and a detection rate of 0.004 to 0.01 ions/pulse. Reconstructions of APT data were performed using IVAS 3.6.6 software, and established reconstruction protocols[8–10] and calibrated using the spacing of the (011) planes imaged within the dataset.[11]

Quantitative analysis on size and dispersion of precipitates is carried out by analyzing the TEM images of the carbon extraction replicas using the Image-pro software. Each precipitate is assumed to be a spherical particle and its radius is calculated from the equivalent area of the precipitate. The analysis of thermodynamic potential for the precipitation of stoichiometric Ti and Nb carbo-nitrides was carried out using Hillert and Staffanson's model for sublattice regular solution.[12,13] Measurement of austenite grain size is performed by EBSD data analysis.[14]

III. EXPERIMENTAL RESULTS

A. *Ti-Nb-Rich Precipitate and Austenite Grain Size in the As-Normalized SMSs*

Figures 1(a) and (b) show the EBSD band contrast map associated with high angle boundaries with misorientation angle above 15 deg indicated by black lines of two SMSs without and with 0.11 wt pct Nb after normalizing at 1323 K (1050 °C), respectively. The thick line delineates the prior austenite grain boundaries. Statistical analysis of the austenite grain diameter in SMSs and Nb-SMSs is given in Figures 2(a) and (b), respectively. In Nb-SMSs, the distribution of the austenite grain diameter is unimodal and the average austenite grain diameter is measured to be 28 ± 9.8 μm. In SMSs, although the average austenite grain diameter is measured to be 44 ± 18.7 μm, an irregular distribution of austenite grain diameter is observed with high frequency of coarse austenite grains. This observation indicates that significant coarsening of austenite grains to 60 to 100 μm occurs in SMSs after normalizing so that coarse grains tend to annex fine grains.[15] By comparison, a uniform distribution of fine austenite grains is observed in SMSs-Nb. The effect of 0.11 wt pct Nb addition thus prevents coarsening of austenite grains during solution treatment.

The effect of Nb addition on preventing austenite grain coarsening could be attributed to Zener pining of grain boundaries by Nb carbo-nitrides and/or solute drag effect of Nb in solution. TEM was used to characterize the precipitates in a normalized Nb-SMSs sample. A high number density and uniform dispersion of precipitates were observed. Figure 3(a) shows a typical TEM image of carbon extraction replica of precipitates. Results for a statistical analysis on the size distribution of the precipitates are given in Figure 4. The average precipitate diameter is found to be 24 ± 8 nm. EDS analysis of the chemical composition of these precipitates shows X-ray signals characteristic of Ti and Nb, as shown in Figure 3(b). Composition mapping of the precipitates using STEM-EELS is shown by the color map in Figure 3(c). It can be seen that the precipitates have a core that is Ti rich, or in some cases Ti and Nb rich, and a shell that is Nb rich. This observation is consistent with previous reports of epitaxial growth of niobium carbo-nitrides on pre-existing titanium nitride.[16,17] The content of Nb in solution was measured using APT. Figure 5(a) shows the Nb atomic map of the as-normalized sample. The distribution of Nb atoms is observed to be uniform. This is confirmed by the 1st nearest neighbor (1NN) distribution of Nb atoms, which matches the distribution of randomized data (Figure 5(b)). The retained solute niobium is analyzed to be 0.08 wt pct, which indicates that 0.03 wt pct niobium was consumed to promote Nb(C,N) epitaxial growth on pre-existing (Ti, Nb)N particles during solution treatment at 1323 K (1050 °C) and upon air cooling to room temperature.

Figure 6 gives the calculation results of the thermodynamic potential for precipitation of stoichiometric Ti and Nb carbo-nitrides using Hillert and Staffanson's model for sublattice-regular solution in a Fe-C-Mn

Table I. Chemistries of 13 Wt Pct Cr Steels

Steel Grade	C	Si	Mn	P	S	Cr	Ni	Mo	N	Nb	Ti
SMSs											
Wt pct	0.020	0.42	0.51	0.016	0.004	12.59	5.01	1.90	0.013	—	0.0062
At pct	0.093	0.84	0.52	0.029	0.007	13.49	4.73	1.10	0.052	—	0.0072
Nb-SMSs											
Wt pct	0.022	0.41	0.48	0.016	0.006	12.91	5.16	2.05	0.010	0.11	0.0043
At pct	0.102	0.82	0.49	0.029	0.010	13.84	4.88	1.19	0.040	0.066	0.0050

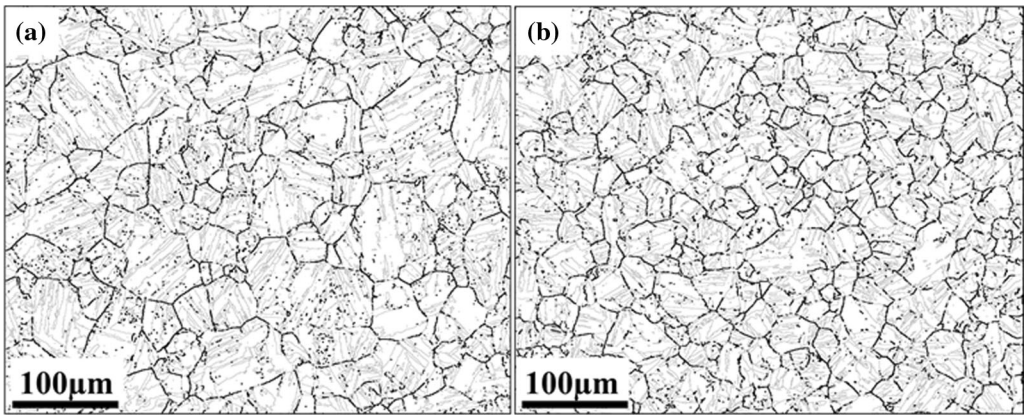

Fig. 1—EBSD band contrast maps comparing austenite grains in (*a*) SMSs without Nb and (*b*) Nb-SMSS. The black line associated with high angle misorientation boundaries above 15 deg delineates the prior austenite grain boundaries.

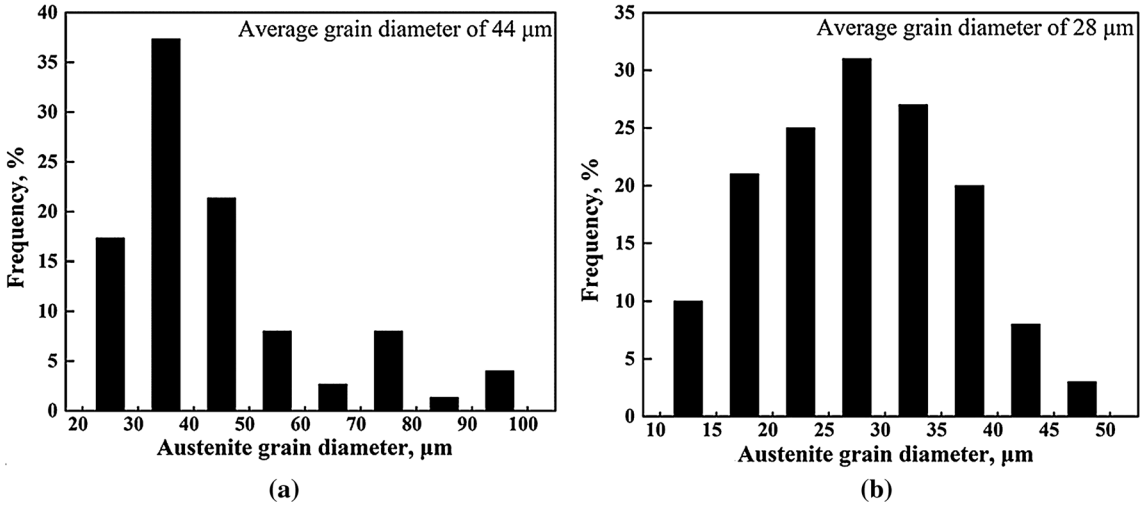

Fig. 2—Austenite grain diameter distribution in two steels: (*a*) SMSs (*b*) Nb-SMSs.

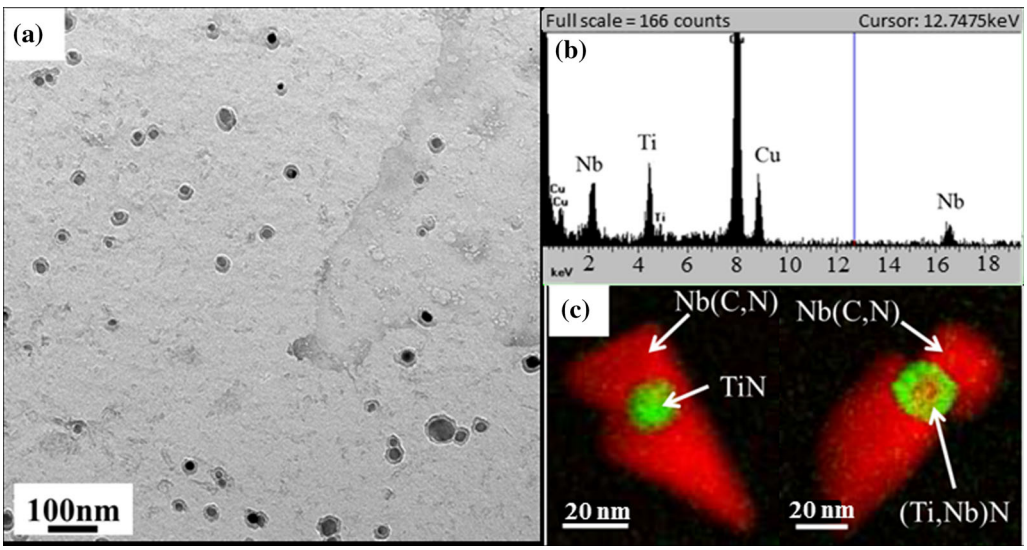

Fig. 3—(*a*) TEM image of carbon extraction replica showing precipitates in Nb-SMSs normalized at 1323 K (1050 °C), (*b*) typical EDS spectrum for precipitates in (a) showing X-ray signals characteristic of Ti and Nb, (*c*) EELS mapping analysis of the composite precipitates chemistry; the red indicates Nb, and green represents Ti (Color figure online).

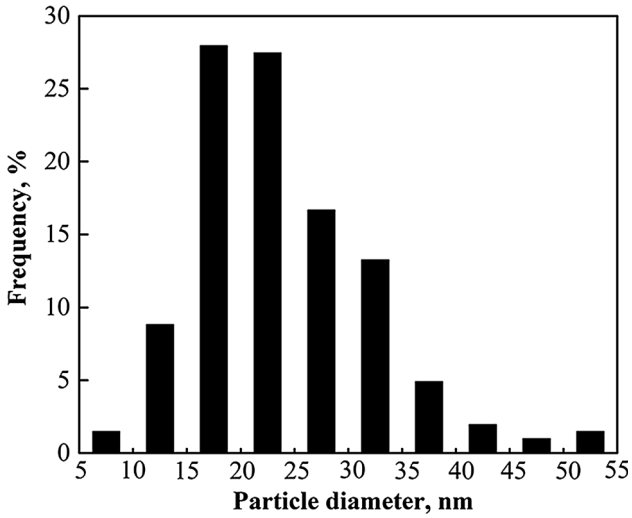

Fig. 4—Statistical analysis of precipitate size distribution in as-normalized Nb-SMSs sample.

system with same content of interstitial elements (C and N) and microalloying elements (Nb and Ti) as in Nb-SMSs. From Figure 6, it is seen that TiN precipitates at a relatively high temperature [*i.e.*, above 1473 K (1200 °C)]. Due to the over-stoichiometric ratio of N to Ti in the steel, excessive N combines with Nb at such high temperatures, resulting in (Ti, Nb)N in the core of the precipitates, as shown in Figure 3(c). Due to a lower thermodynamic potential for precipitation,[18] NbC starts precipitation below 1473 K (1200 °C). The growth of NbC epitaxially on pre-existing (Ti,Nb)N particles results in Nb(C,N) forming the cap of the precipitates, as shown in Figure 3(c). Previous work by Subramanian *et al.*[16] has shown that strain-induced precipitation of NbC carbide requires substantial undercooling in only Nb microalloyed steel, due to the sluggish nucleation of NbC. Conversely, epitaxial growth of NbC on pre-existing TiN particles was reported to occur at the equilibrium precipitation temperature for NbC with negligible undercooling in Ti + Nb microalloyed steel.[16] Pre-existing well-dispersed TiN particles therefore act as the substrate for epitaxial growth of Nb(C, N) at equilibrium temperature, eliminating the nucleation step involved in Ti free steels.

B. *Occurrence of Nb(C, N) Atomic Clusters During Tempering and Its Contribution to Strengthening*

Tempering normalized martensite above the A_{c1} temperature to obtain an adequate volume fraction of reversed austenite is essential for restoration of toughness in super martensitic stainless steel.[2,5,6] However, the increase in toughness brought about by reversed austenite is inevitably at the cost of strength. This effect can be compensated by promoting clustering and precipitation hardening of Nb(C, N) during tempering. A significant increment (160 MPa) in strength is obtained in Nb-SMSs after tempering at 873 K (600 °C) for 2 hours compared with as normalized Nb-SMSs,[5,6] as shown in the histogram in Figure 7.

Clarification of the mechanism underlying this observed strength increase is attempted through characterization of precipitates/atom clusters in Nb-SMSs tempered at 873 K (600 °C) using TEM and APT. TEM examination of the microstructure of Nb-SMSs tempered at 873 K (600 °C) shows high density of dislocations, characteristic of martensite. A typical TEM image is shown in Figure 8. No evident precipitate is seen in the matrix or at dislocations. Figure 9(a) shows an APT reconstruction of tempered Nb-SMSs, depicting C atoms and a set of iso-concentration surfaces that encompass regions of the data containing more than 1.5 at. pct Nb. There have been several proofs recently that linear segregations of solutes observed in APT can be attributed to dislocations.[19–22] Here, Nb-rich features, below 5 nm in size, appear to be aligned along dislocations like those observed in Figure 8, which are marked 1, 2, and 3 in Figure 9(a). At this length scale, and due to limitations in the spatial resolution of APT, it is impossible discern whether these features are atomic clusters, or ordered precipitates, but considering that their compositions are not that of any thermodynamically stable phase, they are likely to be transient structures and will be referred to herein as clusters. The size and dispersion of these clusters are considerably finer than the (Ti,Nb)N-Nb(C, N) composite precipitates discussed in Section III–A, which form at high temperature and thus exist prior to tempering. The fine Nb-rich clusters shown in Figure 9(a) occur within matrix volumes found in-between the larger (Ti,Nb)N-Nb(C,N) composite precipitates. Figures 9(b) and (c) show the distribution of C and Nb by mapping C, and Nb + NbN complexes, respectively. The arrangement of Nb, C, and N atoms suggests co-clustering at dislocations. A composition profile can be computed based on the position of the iso-concentration surface following the protocol known as proximity histogram or proxigram introduced by Hellman.[23] An example of a proxigram is shown in Figures 9(d) and (e), which map the composition profile across the interface between the matrix and the clusters sitting at dislocation 1. While the enrichment of Nb, Cr, C, and N is clearly seen, no apparent excess of Mo is observed. Concentrations of the alloying elements Cr, Nb, C, and N at the core of the Nb-rich clusters are given in the table in Figure 9(f). Due to potential overlap with matrix atoms in the APT data, the Fe content (and to a lesser extent the Cr content) and absolute solute measurements may not be reliable. However, the local excess of solute can still be determined.[24,25]

Danoix *et al.*[26] investigated the precipitation sequence of NbC and NbN at 873 K (600 °C) in model HSLA steels with low and high N content using APT. It was reported that the precipitation process of NbC in the quenched and aged HSLA steels with low N is not direct but through a complex kinetics path, *i.e.*, C and Nb atoms segregate first in the form of isostructural diffuse atmospheres, with a C:Nb atomic ratio of 2.8 after aging for 5 minutes. This ratio decreases to 1.2 after 10 minutes aging with the presence of incoherent metastable transition (Fe, Nb)C particles. With an increase in aging time to 30 minute, diffuse solute atom

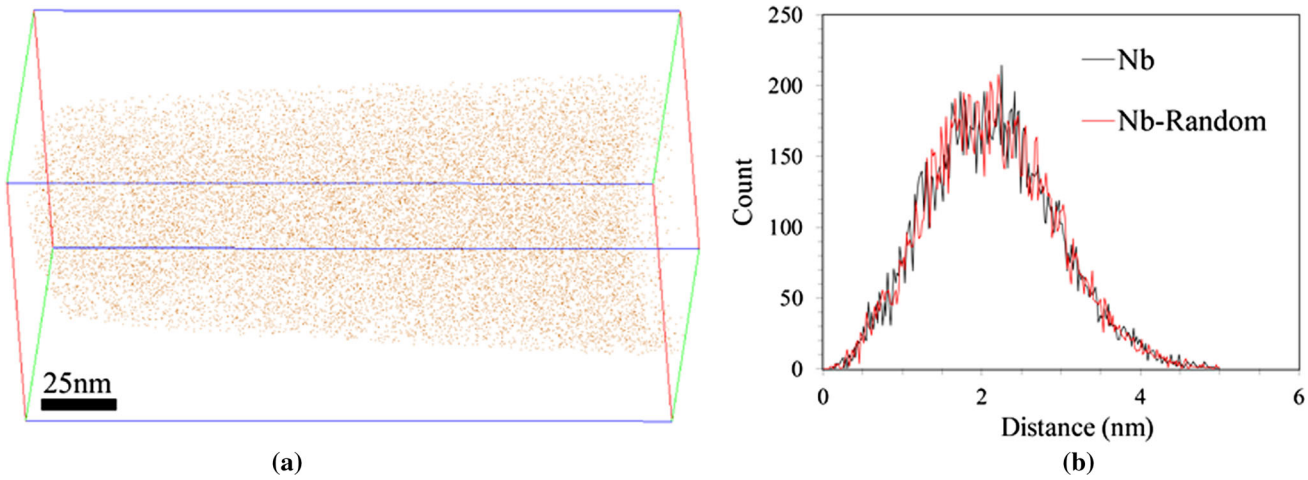

Fig. 5—(*a*) 3D APT atom map and (*b*) 1NN distribution of retained Nb in as-normalized Nb-SMSs (Color figure online).

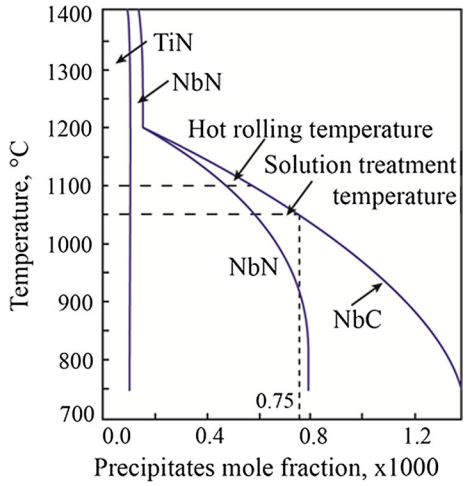

Fig. 6—Thermodynamic calculation of cumulative mole fraction of Ti and Nb carbo-nitrides as a function of temperature in Fe-C-Mn system with 0.0043Ti, 0.11Nb, 0.022C, and 0.01N (in wt pct).

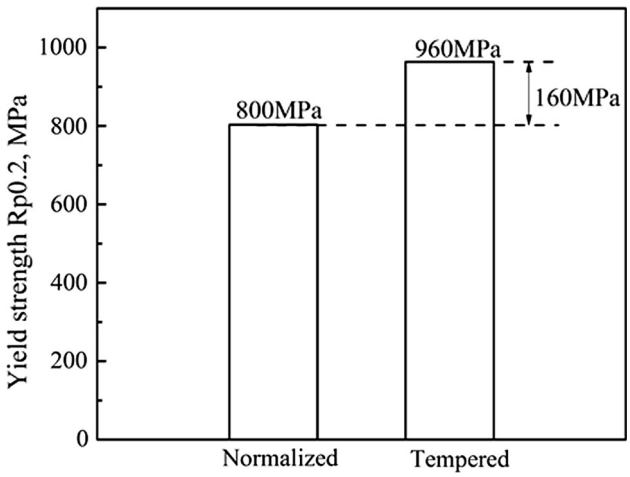

Fig. 7—Yield strength of Nb-SMSs showing the strength increase of 160 MPa by tempering.

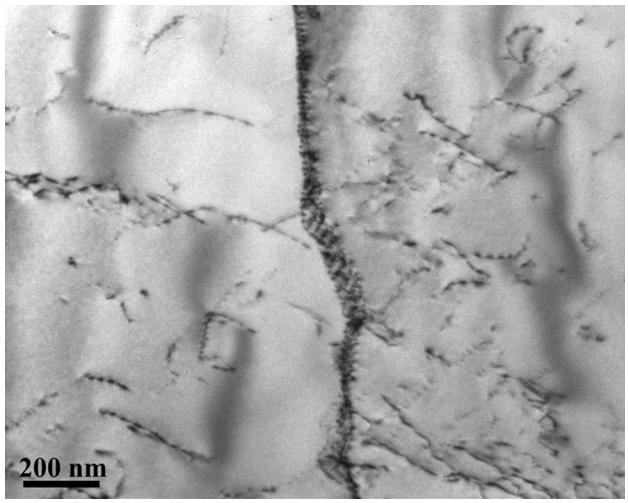

Fig. 8—A typical TEM image showing the presence of dislocations in Nb-SMSs tempered at 873 K (600 °C).

atmospheres were no longer observed and (Fe,Nb)C transforms into NbC. By comparison, no Nb and N (carbon free) diffuse atmospheres were observed in the high N containing steel after aging for 5 minutes. Instead, fully coherent GP zones of monoatomic NbN platelets occurred, which were assumed to act as the nuclei for NbN and NbCN precipitates lying on $\{001\}_{\text{ferrite}}$ planes, with a Baker-Nutting orientation relationship with ferrite matrix for prolonged aging.[27,28] The initial high C-to-Nb ratio was interpreted by the high mobility of C compared to Nb. Bemont[29,30] reported only C but not Nb segregation at dislocations at early stage of aging. The author's previous work on the compositional analysis of precipitates formed in Nb-SMSS tempered at 973 K (700 °C) for 2 hours has confirmed that final stage of Nb(C,N) precipitates do not contain Cr and Fe.[5] The slower kinetics resulting from tempering at lower temperatures of 873 K (600 °C) for 2 hours leads to formation of transient atom co-clusters associated with local excess of Cr, Nb, C, and N in the present study. Except for

(Ti,Nb)N-Nb(C, N) composite precipitates discussed in Section III–A, careful TEM observation did not find any evidence for the existence of fine Nb(C,N) precipitates, which strongly support that these atom co-clusters have iso-structure with matrix.

By comparison, Cr- and Mo-rich precipitates occur in SMSs without Nb during tempering at 873 K (600 °C).[6] Figures 10(a) and (d) show reconstructed APT data with two types of Cr- and Mo-rich precipitates, in the matrix of tempered SMSs without Nb. Proxigrams given in Figures 10(b) and (e) show composition profiles between the precipitates and tempered martensite matrix. The composition, as measured from the plateaus of two precipitates, is given by the respective tables in Figures 10(c) and (f). Composition analysis suggests that the precipitates are Cr- and Mo-rich carbides. Previous TEM work has found that Nb addition suppresses the occurrence of Cr- and Mo-rich carbide precipitation in Nb-SMSs upon tempering at 873 K (600 °C).[6] This is attributed to a higher affinity of Nb for C than that of Cr and Mo for C, such that Nb combines preferentially with C to form NbC clusters. Such clusters are confirmed by APT observation, as shown in Figure 9. Although Cr is noted to show enrichment along with Nb, C, and N as well in those clusters, the magnitude of Cr enrichment is significantly greater for the precipitates shown in Figure 10(a).

IV. DISCUSSION

A. *Control of Austenite Grain Size by (Ti,Nb)N-Nb(C, N) Composite Precipitate Engineering*

Austenite transformation occurs upon reheating from room temperature to 1323 K (1050 °C) for the homogenization treatment. Austenite grains grow and coarsen during maintaining at 1323 K (1050 °C) for 30 minutes. The driving force F_{DRI} for grain coarsening is capillarity, which equals $2\gamma/R$, where γ is the surface energy and R is the radius of austenite grain. The Zener pinning pressure F_{PIN} brought about by (Ti,Nb)N-Nb(C,N) composite precipitates counteracting capillarity driven driving force for grain coarsening in Nb-SMSs is $2\pi r^2 N\gamma$, where r is precipitate radius, N is the number of particles per volume and γ is austenite grain boundary surface energy.[31,32] For given isothermal treatment temperature and time, the magnitude of austenite grain coarsening depends on boundary migration velocity of v, which is generally expressed as

$$v = MF_{\mathrm{net}} \qquad [1]$$

where F_{net} is the net driving force for austenite grain boundaries migration and equals $F_{\mathrm{DRI}} - F_{\mathrm{PIN}}$, M is grain boundary mobility and according to Cahn's theory of solute drag $\frac{1}{M} = \frac{1}{M_i} + \frac{\alpha C}{1+\beta^2 v^2}$ (M_{i} is the intrinsic grain boundary mobility and C is the solute Nb concentration[33–35]).

While (Ti,Nb)N-Nb(C,N) composite precipitates resulting from epitaxial growth of Nb(C,N) on pre-existing (Ti,Nb)N particles exert a Zener pinning pressure on austenite grain boundary, Nb remaining in solution decreases the mobility of austenite grain boundary. Maalekian *et al.*[36] predicted austenite grain coarsening kinetics during continuous heating and subsequent isothermal soaking and compared with the experimentally determined austenite grain sizes in a Ti-Nb microalloyed steel. They reported that limiting austenite grain size is reached rapidly after reheating (less than 1 minute).

Therefore, it is considered in the present study that the Zener limiting austenite grain size is reached after holding at 1323 K (1050 °C) for 0.5 hours in Nb-SMSs, which indicates $2\gamma/R = 2\pi r^2 N\gamma$, resulting in

$$R = 1/(\pi r^2 \cdot N) \qquad [1]$$

in which N can be replaced by $N = 1/\lambda^3$ or $N = f/((4/3)\pi r^3)$.

$$R = \lambda^3/(\pi r^2) \text{ or } R = 4r/(3f) \qquad [2]$$

where λ is inter-particle spacing and f is volume fraction of (Ti,Nb)N-Nb(C,N) composite precipitates.

It is assumed that the microalloying elements Ti and Nb combine with interstitial C and N during precipitation according to their stoichiometric ratio of atomic weights. All Ti exists in the form of precipitates. The amount of precipitated Nb in the normalized Nb-SMSs is calculated to be 0.03 wt pct based on APT results given in Figure 5 for a given total Nb content of 0.11 wt pct. For precipitated Nb content of 0.03 wt pct and Ti content of 0.0043 wt pct, the total mole fraction of (Ti,Nb)N-Nb(C,N) composite precipitates in the normalized Nb-SMSS sample is calculated to be 0.00046. Taking into account the molar volume of the precipitate and Fe matrix, the volume fraction of (Ti,Nb)N-Nb(C,N) composite precipitates is calculated to be 0.00083 (see-Appendix A). For the measured composite precipitate average diameter of 24 ± 8 nm, the inter-particle spacing of (Ti,Nb)N-Nb(C,N) composite precipitate is calculated to be 205 ± 68 nm. However, the Zener limiting austenite grain size during solution treatment depends on the volume fraction of (Ti,Nb)N-Nb(C,N) composite precipitate at 1323 K (1050 °C) for the given inter-particle spacing set out originally by TiN. The amount of precipitated Nb upon cooling from 1323 K (1050 °C) to room temperature depends on the inter-particle spacing of pre-existing TiN particles, the diffusion distance of Nb ($\sqrt{Dt}$, where D is diffusion coefficient and t is time), and the cooling rate.[13,37] Due to the low diffusion rate of Nb in relatively dislocation-free austenite and the fast cooling rate associated with the small samples (10 × 10 × 20 mm) upon air cooling, the amount of Nb precipitated during air cooling from 1323 K (1050 °C) to room temperature is negligible. Thus, the calculated volume fraction of 0.00083 (Ti, Nb)N-Nb(C,N) composite precipitates is assumed to be equal to the fraction formed at 1323 K (1050 °C). For the inter-particle spacing of 205 ± 68 nm, the Zener limiting austenite grain diameter is calculated to be 38 ± 13 μm for this case, which agrees with the

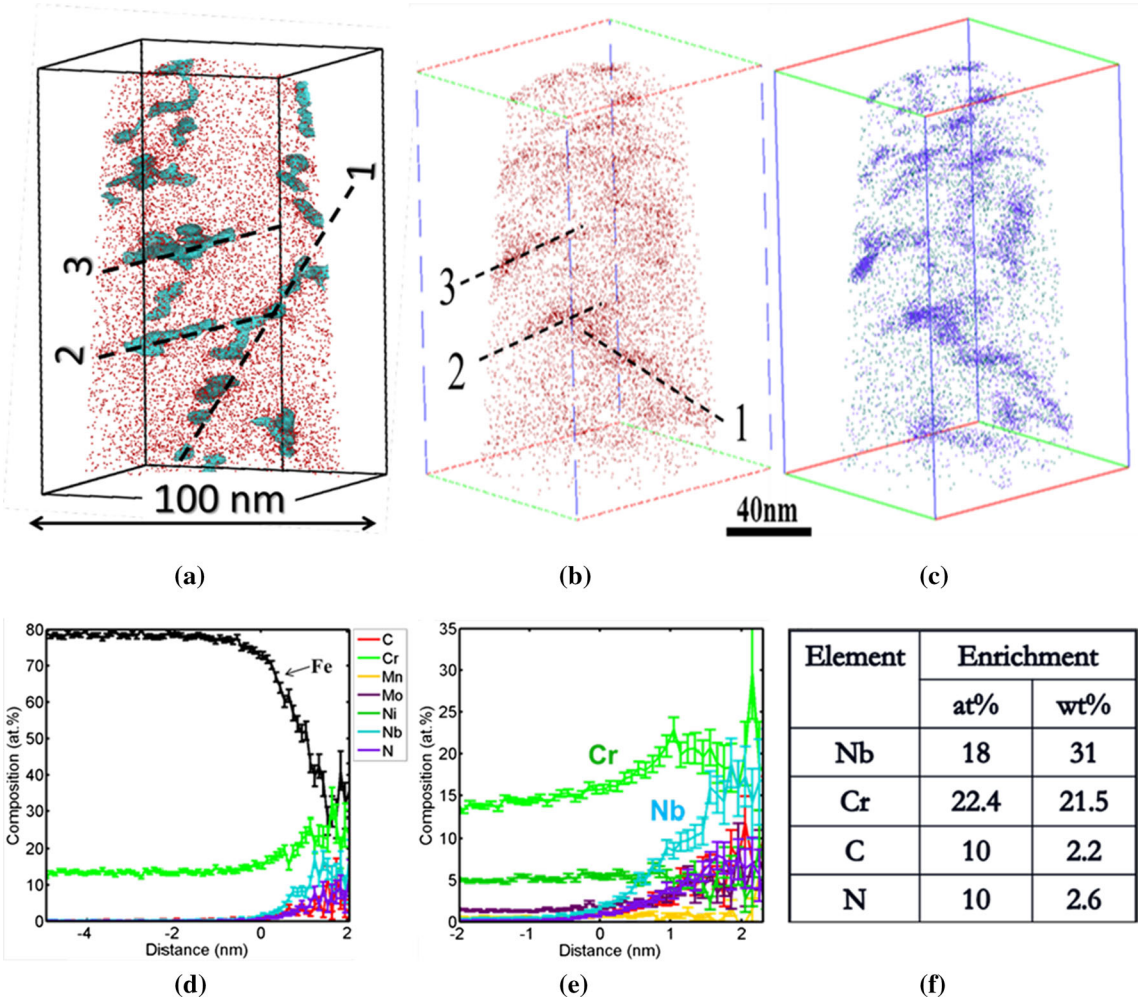

Element	Enrichment	
	at%	wt%
Nb	18	31
Cr	22.4	21.5
C	10	2.2
N	10	2.6

(f)

Fig. 9—3D APT reconstruction of Nb-SMSs, normalized at 1323 K (1050 °C) and tempered at 873 K (600 °C) for 2 h. (*a*) C atom map (red) and 1.5 at. pct Nb isosurfaces (green) along dislocations. Atomic maps of (*b*) C (red) and (*c*) Nb atoms (green) and NbN (blue) complexes, showing partitioning along dislocations. (*d*) and (*e*) proxigram showing concentration profile across the interface between matrix/clusters at dislocation-1. (*f*) average solute composition at the core of the Nb-rich clusters (Color figure online).

austenite grain size distribution observed in as-normalized Nb-SMSS, as shown in Figure 2(b).

It is worth noting that, based upon Eq. [1], the limiting austenite grain radius has a reciprocal relationship with the product of the number of particles per volume and the square of the particle radius. Both a high number density (*i.e.*, short inter-particle spacing) and a large particle radius are important to reduce the Zener limiting austenite grain size. Epitaxial growth of Nb(C,N) on pre-existing (Ti,Nb)N particles at the equilibrium temperature allows independent control over the inter-particle spacing and the particle radius to prevent austenite grain coarsening at high temperature.[38] Indeed, while the inter-particle spacing can be controlled through the TiN particle dispersion, the radius of the particle can be increased through epitaxial growth of Nb carbo-nitrides on pre-existing TiN particles.

Figure 11(a) shows the plot of limiting austenite grain diameter as a linear function of inter-particle spacing for a given volume fraction of 0.000165 for TiN and 0.00083 for (Ti,Nb)N-Nb(C,N) precipitates, as obtained for the normalized Nb-SMSs in the present study. For two different arbitrary inter-particle spacing values of 200 and 500 nm, the radii of pre-existing TiN particles formed above 1473 K (1200 °C) are calculated to be 6.8 and 17 nm, respectively, and the corresponding limiting austenite grain size values are calculated to be 110 and 275 μm, respectively. The significant difference between these two values shows that controlling the inter-particle spacing through promoting a fine TiN particle dispersion is a key factor in reducing the Zener limited austenite grain size. Control of the short inter-particle particle spacing of the TiN precipitate requires control of Ti and N to promote TiN precipitation in solid austenite at lower temperature rather than in liquid at higher temperature. Nagata *et al.*[39] reported that a hypostoichiometric ratio of Ti to N as contained in Nb-SMSs in the present study is favorable to promote finely dispersed TiN particles. For the same inter-particle spacing, the particle radius increase resulting from epitaxial growth of Nb(C, N) on pre-existing TiN particles decreases the limiting austenite grain size values. Figure 11(b) expands on this relation by plotting

the limiting austenite grain diameter as a function of precipitate radius [obtained at different austenization temperatures ranging from 1473 K to 1323 K (1200 °C to 1050°C)] for the inter-particle spacing of 200 nm. The radius of the particle is increased from 6.8 nm for just the TiN of 0.000165 in volume fraction to 11.66 nm for the (Ti,Nb)N-Nb(C,N) precipitates of 0.00083 in volume fraction. The resulting limited austenite grain size is significantly reduced from 110 μm for just the TiN to 37 μm for the (Ti,Nb)N-Nb(C,N). Therefore, it is clear that high Nb design to promote adequate growth of NbC on pre-existing TiN particles is also essential to obtain a fine grain size in ultralow carbon super martensitic stainless steel.

B. *Mechanism of Nb-Rich Atomic Cluster Strengthening*

The thermodynamic potential for precipitation of Nb(C,N) in Nb-SMSs during tempering at 873 K (600 °C) is determined by the chemical supersaturation of 0.08 wt pct Nb as measured by APT in the matrix.[40,41] The kinetics of precipitation can be accelerated significantly by high density of dislocations in the as-normalized martensite microstructure, through both lowering the nucleation activation barrier (estimated to be by a factor of ~100 in comparison with homogeneous bulk nucleation[41,42]) and promoting fast diffusion along dislocations. The segregation of Nb, C, and N solute atoms to dislocations, resulting from their elastic strain field, is of importance for Nb(C,N) precipitate nucleation and growth. Nb(C,N) can either grow on pre-existing (Ti,Nb)N-Nb(C,N) composite precipitates or form new precipitates of Nb(C,N) on dislocations during tempering. The balance depends on a combination of the inter-particle spacing of the (Ti,Nb)N-Nb(C,N) composite precipitates, the Nb diffusion rate along dislocations, and the nucleation rate of NbC at dislocations during tempering.[41]

The magnitude of precipitation strengthening depends on the size and the volume fraction of precipitates, as well as the nature of the interaction of the particles with dislocations. For coarse hard particles incoherent with the matrix, it is generally accepted that precipitation strengthening is by the Orowan looping mechanism. Similar to calculations carried out by the other investigators,[43,44] a strength increase arising from TiN of 0.000165 in volume fraction and (Ti,Nb)N-Nb(C, N) precipitates of 0.00083 in volume fraction, with the inter-particle spacing of 205 nm in the as-normalized Nb-SMSS sample is calculated to be 33 MPa and 53 MPa respectively, using Ashby–Orowan model of dislocations bypassing particles (see-Appendix B).[45] It is shown that the strength increase by TiN precipitates is marginal, as is that by (Ti,Nb)N-Nb(C, N) composite precipitates despite the increase in the precipitate size. This is attributed to the large inter-particle spacing, determined originally by the (Ti,Nb)N particles.

The significant increase in yield strength of 160 MPa is gained by tempering to promote a high number density of fine Nb(C, N) clusters, acting to pin/impede dislocations. Cairney, Ringer, and co-workers[43,46–48] reported similar increase in yield strength as obtained in the present work (165 MPa) in a Nb microalloyed HSLA steel containing comparable amounts of Nb and C (0.084 wt pct Nb and 0.03 wt pct C) to the current Nb-SMSs steel (both contain a 0.08 wt pct Nb in solid solution before aging). It is considered that Nb(C,N) atom clusters obtained in the present Nb-SMSs are aggregates of solute Nb as substitutional atom with the same structure as the matrix phase of ferrite and high concentration of C and N as interstitial atoms.[47] The strengthening of Nb(C,N) atom clusters is reported to be by order strengthening.[47,49,50] Shrestha *et al.*[48] calculated Nb solution strengthening of a 31 MPa yield strength increase for 0.08 wt pct Nb. In order to evaluate the order strengthening of Nb(C,N) atom clusters, the volume fraction of Nb(C, N) clusters is estimated from composition analysis of the APT data based on the assumption of Nb(C,N) clusters having the same crystallographic structure as the ferrite phase, even though there is uncertainty in absolute value of cluster concentration measurement by APT due to its local magnification effect. Taking an average retained solute Nb content of 0.01 wt pct (0.006 at. pct) in a matrix free of Nb(C, N) clusters, and the peak concentration of 31 wt pct (18 at. pct) Nb in Nb(C,N) clusters, also measured by the APT (Figure 9(a)), the volume fraction of Nb(C,N) clusters is estimated to be 0.00233 based on a mass balance calculation. For order strengthening, the passage of a dislocation through a Nb(C,N) cluster requires an increase in shear stress to produce an interphase boundary with an associated disordering energy. Based on Ardell's model of precipitation hardening by shearing mechanism,[50] the yield strength increase from order strengthening is calculated to be 170 MPa (see Appendix C). The actual yield strength increment of 160 MPa in Nb-SMSs from the as-normalized state to the as-tempered state equals the order strengthening minus a decrease in yield strength caused by the presence of reversed austenite and dislocation recovery due to tempering above A_{c1}. Nevertheless, due to the retardation effect of Nb on reversed austenite formation kinetics, the volume fraction of reversed austenite obtained in Nb-SMSs after tempering at 873 K (600 °C) for 2 hours is very small, beyond the resolution of XRD techniques.[5,6] Therefore, its effect on decreasing the yield strength is negligible compared to the cluster strengthening increment.

By comparison, the volume fraction of Nb(C, N) second-phase particles that can be obtained from precipitation of 0.07 wt pct Nb out of the total 0.08 wt pct solute Nb retained in the as-normalized Nb-SMSs is calculated to be 0.00155. For precipitation strengthening by the Ashby–Orowan mechanism, where dislocation bow and bypass discrete hard Nb(C,N) particles, the yield strength increase is calculated as a function of precipitate diameter (or inter-particle spacing) for a given volume fraction of 0.00155, as shown in Figure 12. According to this calculation, the same strength increment as can be obtained by order strengthening of Nb(C,N) clusters (170 MPa) can be achieved by dislocation bypassing of Nb(C, N) precipitates for a precipitate diameter of 6.6 nm with inter-precipitate

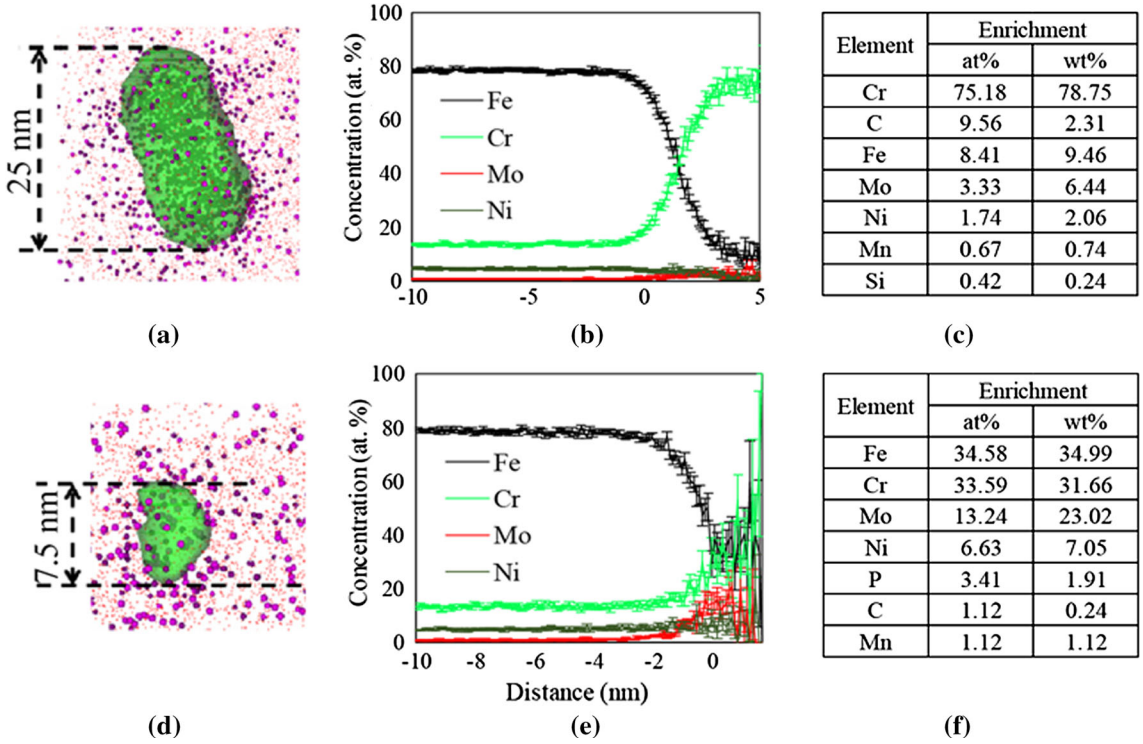

Element	Enrichment	
	at%	wt%
Cr	75.18	78.75
C	9.56	2.31
Fe	8.41	9.46
Mo	3.33	6.44
Ni	1.74	2.06
Mn	0.67	0.74
Si	0.42	0.24

Element	Enrichment	
	at%	wt%
Fe	34.58	34.99
Cr	33.59	31.66
Mo	13.24	23.02
Ni	6.63	7.05
P	3.41	1.91
C	1.12	0.24
Mn	1.12	1.12

Fig. 10—Composite diagram showing 3D APT reconstruction maps of Cr- and Mo-rich precipitates in SMSs without Nb tempered at 873 K (600 °C) for 2 h (*a* and *d*); and chemical composite profile normal to interface between precipitates and martensite matrix in linear (*b* and *e*) and chemical composition measured from plateau (*c* and *f*) (Color figure online).

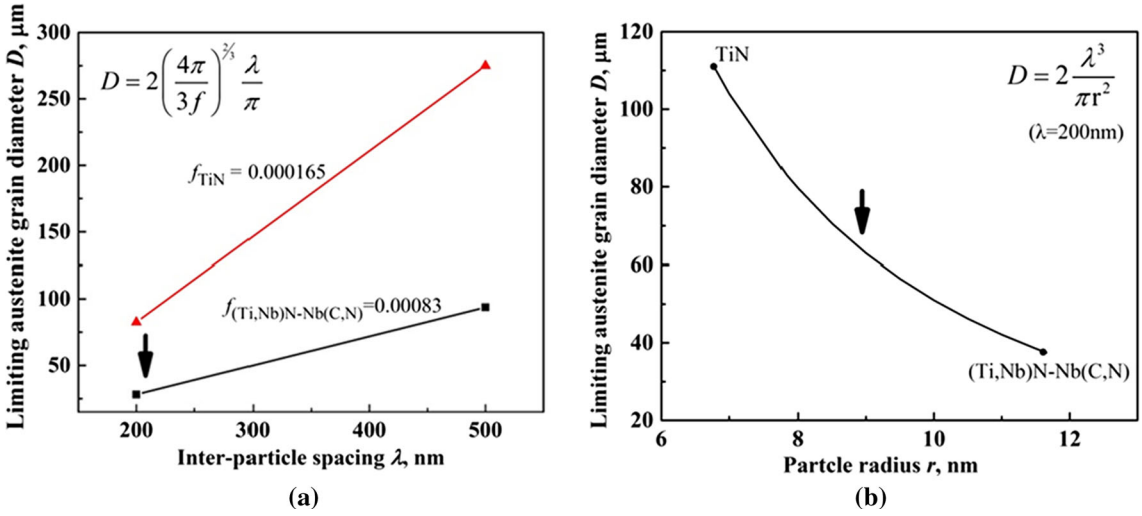

Fig. 11—(*a*) limiting austenite grain diameter as a function of inter-particle spacing in the range of 200 to 500 nm for a given volume fraction of 0.000165 for TiN and 0.00083 for (Ti,Nb)N-Nb(C,N) precipitates obtained in normalized Nb-SMSs with chemistry of 0.0043 pct Ti, 0.01 pct N, 0.022 pct C, and 0.011 pct Nb (wt pct), (*b*) limiting austenite grain size as a function of particle radius for given average inter-particle spacing of 200 nm.

spacing of 45 nm, as indicated by dashed lines in Figure 12.

In principle, a further increase in the yield strength of Nb-SMSs can be obtained by promoting a dispersion of Nb(C,N) precipitates. Pereloma reported bimodal peaks of hardness associated with pre-precipitation atomic co-clusters and discrete precipitates, respectively, with the second peak higher than first peak, in a Fe-Ni-Mn-Ti-Al maraging steel after aging at 823 K (550 °C) for prolonged time.[51,52] Whereas in the abovementioned work of Shrestha and Xie *et al.*,[43,47] with increasing aging time, the maximum increase of 165 MPa in yield strength was found to be associated with the occurrence of the Nb(C,N) atomic clusters, and no further increase in yield strength after prolonged aging times due to discrete Nb(C,N) precipitation was

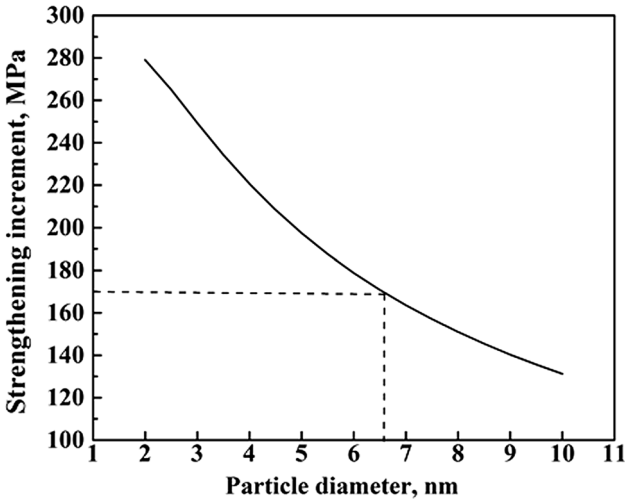

Fig.12—Precipitation strengthening as a function of Nb(C, N) particle diameter for a given volume fraction of 0.00155.

observed. As the strengthening mechanism in Nb-SMSs in the present work is by Nb(C,N) atom clusters as well, the precipitation hardening behavior in Nb-SMSs is considered to be similar to that in the HSLA steel reported by Xie and Shrestha *et al.*[43,47] In their work, the same maximum hardness increment was obtained after aging at 798 K (525 °C) for 24 hours, 973 K (700 °C) for 4 minutes, and 1073 K (800 °C) for 20 seconds due to occurrence Nb(C, N) atom clusters, indicating that the peak hardness caused by Nb(C,N) atom clusters is independent of aging temperatures and is a function of aging time.[47] Therefore, aging Nb microalloyed steel to peak hardness can be treated as a thermally activated process and Shrestha's analysis on the kinetics of the process using Arrhenius equation is reproduced here[47]

$$k = k_0 e^{\left(-\frac{Q}{RT}\right)} \quad [3]$$

$$\ln k = \ln k_0 - \frac{Q}{RT}, \quad [4]$$

where k is the rate constant and is a function of the reciprocal of time for peak hardening at each tempering temperature T; k_0 is the pre-exponential factor; Q is the activation energy of aging required for the steel to reach peak hardness by Nb(C,N) atomic clusters; and R is universal gas constant.

Considering times of 20 seconds at 1073 K (800 °C) and 24 hours at 798 K (525 °C) for peak hardening from Shrestha's results,[47] the activation energy for the overall transformation process including nucleation and growth is calculated to be 216.7 kJ/mol, based on which the aging time for peak hardness at 873 K (600 °C) is predicted to be 1.5 hours. A high concentration of vacancies and dislocations originating from the high temperature and the rapid cooling leads to a faster substitutional diffusion of Nb, thereby resulting in a reduced activation energy and shorter aging time to reach peak hardness. On the contrary, a low concentration of defects in the microstructure will lead to a longer aging time to reach peak hardness. It is assumed that the density of vacancy and dislocation in normalized Nb-SMSs by air cooling is lower than that in water-quenched microstructure of Shrestha's steel, the increase of 160 MPa in yield strength obtained in Nb-SMSs after tempering at 873 K (600 °C) for 2 hours in present work is considered to be close to peak value of aging strengthening. It is proposed that further extension in aging time at 873 K (600 °C) beyond 2 hours will promote formation of discrete Nb(C,N) second-phase precipitates with lower volume fraction and number density when compared with Nb(C,N) atomic clusters. For strengthening by Ashby-Orwan dislocation bypassing Nb(C,N) precipitates, increase in volume fraction of the Nb(C,N) precipitates at the expense of Nb(C,N) clusters would not be large enough to compensate for the decrease due to increased distance between the particles to dislocation migration, thereby leading to the decrease in strengthening effect. Pereloma[51] and Ringer[53] reported that atomic cluster strengthening by shearing mechanism offers a significant strength increment without compromising ductility and toughness when compared with precipitates strengthening by Ashby–Orowan dislocation looping mechanism, where micro-cracks will be initiated from dislocation pile-ups. However, in present study, the complex combination of cluster, dislocation recovery, and the presence of retained austenite makes it difficult to sort out the sole effect of cluster on ductility and toughness of Nb-SMSs.

V. CONCLUSIONS

The present work clarifies the functional roles of Nb in normalized and tempered Ti-bearing SMSs through characterization of multi-scale, multi-level Nb-rich precipitates/atomic clusters. The use of TEM and 3D APT elucidates the role of the precipitates/atom clusters in interacting with austenite grain boundaries and dislocations. It is found that:

(1) The effect of 0.11 wt pct Nb addition to Ti-bearing SMSs is to promote epitaxial growth of Nb(C,N) on pre-existing (Ti,Nb)N particles during solution treatment at 1323 K (1050 °C), thereby promoting (Ti, Nb)N-Nb(C,N) composite precipitate. Quantitative analysis shows that the effect of (Ti, Nb)N-Nb(C,N) composite precipitate in diameter of 24 ± 8 nm with inter-particle spacing of 205 ± 68 nm originally determined by (Ti,Nb)N particles is to confer Zener limiting austenite grain size of 38 ± 13 μm, which is consistent with experimental observation of austenite grain size distribution in as-normalized Nb-SMSS.
(2) Control of inter-particle spacing by promoting TiN particle dispersion is identified to be the key to increase the Zener pinning pressure at austenite grain boundaries, to prevent grain coarsening of austenite for a given chemistry. Increase in size/volume fraction of precipitates by promoting

epitaxial growth of Nb(C,N) on pre-existing (Ti,Nb)N particles increases the Zener pinning pressure further.

(3) 3D APT characterization of as-normalized Nb-SMSs sample confirmed that 0.08 wt pct solute Nb is retained following the formation of Nb(C, N) during solution treatment (on (Ti,Nb)N) and air cooling to room temperature. Nb(C,N) multi-component atom clusters at dislocations resulting from tempering the normalized Nb-SMSs at 873 K (600 °C) for 2 hours contribute to a yield strength increase of 160 MPa, which is predicted to be close to the maximum strengthening effect.

(4) Retaining solute Nb in the as-normalized Nb-SMSs also suppresses precipitation of Cr- and Mo-rich carbides upon tempering at 873 K (600 °C) by preferentially combining Nb with C and N to form Nb(C,N) atom clusters.

ACKNOWLEDGMENTS

Grateful thanks are expressed to Dr. Gianluigi Botton, Dr. Glynis de Silveira, and Dr. Andreas Korinek for their help on TEM-EELs characterization of the steel sample, and to Dr. Lijun Wang for help on steel sample preparation. The funding support from CBMM, Brazil is gratefully acknowledged.

APPENDIX A

$$f = \frac{V_{MN}}{V_{MN} + V_{Fe}}, \quad [A.1]$$

where V_{MN} is the volume of precipitated MN and V_{Fe} is the volume of ferrite. The volume V of a given mole X of a material can be calculated as

$$V = X\frac{N_a}{N_u}V_u, \quad [A.2]$$

where X is mole of the material; N_a is the Avogadro's number; N_u is the number of atoms per unit cell of the materials (N_u is 4 for MN precipitate and austenite Fe, and 2 for ferritic Fe, respectively); V_u is the volume of the unit cell of the material and cube of the lattice parameter for MN. (Lattice parameter: 0.359 nm for austenite Fe, 0.286 nm for ferrite Fe, 0.425 nm for TiN, 0.443 nm for NbC)

$$X_{MN} = X_M + X_N, \quad \text{where } X_M = \frac{m_M}{P_M}, \quad X_N = \frac{m_N}{P_N}, \quad [A.3]$$

where m is mass of a material and P is the atomic weight of the material.

For assumption of stoichiometric ratio between M and N, $X_M = X_N$.

$$V_{MN} = \left(\frac{m_M}{P_M} + \frac{m_N}{P_N}\right)\frac{N_a}{N_u}V_u = 2\left(\frac{m_M}{P_M}\right)\frac{N_a}{N_{u_{MN}}}V_{u_{MN}}, \quad V_{Fe} = \frac{m_{Fe}}{P_{Fe}}\frac{N_a}{N_{u_{Fe}}}V_{u_{Fe}}, \quad [A.4]$$

Therefore, volume fraction of MN can be calculated by substituting all values in Eq. [A.1].

APPENDIX B

The Ashby–Orowan equation can be expressed as

$$\Delta\sigma_1 = \frac{0.8\,MGb}{2\pi\sqrt{1-\upsilon}\lambda}\ln\left(\frac{x}{2b}\right), \quad [B.1]$$

where M is the Taylor factor, taken as 2.75; υ is the Poisson's ratio, taken as 0.293; G is the Shear modulus of low carbon steel, 79,600 MPa; b is the Burger's vector, 0.248 nm; λ is the inter-spacing of particles on slip plane.

$$\lambda = \frac{1}{2}\sqrt{\frac{2}{3}}\left(\sqrt{\frac{\pi}{f}} - 2\right)d \quad [B.2]$$

$$x = \sqrt{\frac{2}{3}}d,$$

where d is the mean diameter of particle.

For a given volume fraction, f, and precipitate diameter, d, the increment in yield strength can be calculated by substituting all values in Eq. [B.2].

APPENDIX C

The order strengthening from Nb(C,N) atom clusters can be calculated from

$$\Delta\sigma_2 = 0.81M\frac{\gamma}{2b}\left(\frac{3\pi f}{8}\right)^{1/2}, \quad [C.1]$$

where $M = 2$ is the matrix orientation factor; $b = 0.248$ nm is Burger's vector; γ is matrix-cluster interface energy, which is assumed to be 1 J m^{-2}; f is the cluster volume fraction.

For predicted cluster volume fraction of 0.00233 from atom probe data analysis, order strengthening increment is calculated to be 170 MPa.

REFERENCES

1. B. Qin, Z.Y. Wang, and Q.S. Sun: *Mater. Charact.*, 2008, vol. 59, pp. 1096–1100.
2. Y.Y. Song, D.H. Ping, F.X. Yin, X.Y. Li, and Y.Y. Li: *Mater. Sci. Eng. A*, 2012, vol. 527, pp. 614–18.
3. P.D. Bilmes, C.L. Llorente, C.M. Méndez, and C.A. Gervasi: *Corrosion. Sci.*, 2009, vol. 51, pp. 876–81.
4. P.D. Bilmes, M. Solari, and C.L. Llorente: *Mater. Charact.*, 2001, vol. 46, pp. 285–96.

5. X.P. Ma, L.J. Wang, C.M. Liu, and S.V. Subramanian: *Mater. Sci. Eng. A*, 2011, vol. 528, pp. 6812–18.
6. X. Ma, L. Wang, S. Subramanian, and C. Liu: *Metall. Mater. Trans. A*, 2012, vol. 43A, pp. 4475–86.
7. E. Ladanova, J.K. Solberg, and T. Rogne: *Corros. Eng. Sci. Technol.*, 2006, vol. 41, pp. 143–51.
8. B. Gault, M. Moody, J. Cairney, and S.P. Ringer: *Atom Probe Microscopy*, Springer Science, New York, 2012.
9. B.P. Geiser, D.J. Larson, E. Oltman, S.S. Gerstl, D.A. Reinhard, T.F. Kelly, and T.J. Prosa: *Microsc. Microanal.*, 2009, vol. 15 (S2), pp. 292–93.
10. B. Gault, D. Haley, F. de Geuser, M.P. Moody, E.A. Marquis, D.J. Larson, and B.P. Geiser: *Ultramicroscopy*, 2011, vol. 111, pp. 448–57.
11. B. Gault, M.P. Moody, F. de Geuser, G. Tsafnat, A. La Fontaine, L.T. Stephenson, D. Haley, and S.P. Ringer: *J. Appl. Phys.*, 2009, vol. 105, p. 034913.
12. M. Hillert and L.I. Staffanson: *Acta Chemica Scandinavica*, 1970, vol. 24, pp. 3618–26.
13. H. Zou: Ph.D. thesis, McMaster University, Canada, 1991.
14. L. Ryde: *Mater. Sci. Technol.*, 2006, vol. 22, pp. 1297–1306.
15. T. Gladman and F.B. Pickering: *Yield, Flow and Fracture of Polycrystals*, Applied Science Publishers, London, 1982, pp. 141–98.
16. S.V. Subramanian, F. Boratto, J.J. Jonas, C.M. Sellars: *Proc. of Int. Symp. on Microalloyed Bar and Forging Steels*, 1990, pp. 120–36.
17. S.G. Hong, K.B. Kang, and C.G. Park: *Scr. Mater.*, 2002, vol. 46, pp. 163–68.
18. T. Gladman: *Physical Metallurgy of Microalloyed Steels*, The Institute of Materials, London, 1997, pp. 82–87.
19. M. Kuzmina, M. Herbig, D. Ponge, S. Sandlobes, and D. Raabe: *Science*, 2015, vol. 349, pp. 1080–83.
20. G.D.W. Smith, D. Hudson, P.D. Styman, and C.A. Williams: *Philos. Mag.*, 2013, vol. 93, pp. 3726–40.
21. C.A. Williams, J.M. Hyde, G.D.W. Smith, and E.A. Marquis: *J. Nucl. Mater.*, 2011, vol. 412, pp. 100–05.
22. B. Gault, M.P. Moody, J.M. Cairney, and S.P. Ringer: *Mater. Today*, 2012, vol. 15, pp. 378–86.
23. O.C. Hellman, J.A. Vandenbroucke, J. Rüsing, D. Isheim, and D.N. Seidman: *Microsc. Microanal.*, 2000, vol. 6, pp. 437–44.
24. P. Felfer, A. Ceguerra, S. Ringer, and J. Cairney: *Ultramicroscopy*, 2013, vol. 132, pp. 100–06.
25. P. Maugis and K. Hoummada: *Scr. Mater.*, 2016, vol. 120, pp. 90–93.
26. F. Danoix, E. Bémont, P. Maugis, and D. Blavette: *Adv. Eng. Mater.*, 2006, vol. 8, pp. 1202–05.
27. A. Deschamps, F. Danoix, F. De Geuser, T. Epicier, H. Leitner, and M. Perez: *Mater. Lett.*, 2011, vol. 65, pp. 2265–68.
28. M. Perez, E. Courtois, D. Acevedo, T. Epicier, and P. Maugis: *Mater. Sci. Forum*, 2007, vols. 539–543, pp. 4196–4201.
29. Bémont E. PhD. Rouen, Université de Rouen, France, 2003.
30. E. Bémont, E. Cadel, P. Maugis, and D. Blavette: *Surf. Interface Anal.*, 2004, vol. 36, pp. 585–88.
31. M.F. Ashby: *1st Riso Int. Symp. on Metallurgy and Materials Science on Recrystallization and grain Growth in Multi-Phase Particle Containing Materials*, 1980, pp. 325–36.
32. G.S. Rohrer: *Trans. AIME*, 1948, vol. 175, pp. 15–51, by C.S. Smith: *Metall. Mater. Trans. A*, 2010, vol. 41A, pp. 1063–100.
33. J.W. Cahn: *Acta Matell.*, 1962, vol. 10, pp. 789–98.
34. H.S. Zurob, G. Zhu, S.V. Subramanian, G.R. Purdy, C.R. Hutchinson, and Y. Brechet: *ISIJ Int.*, 2005, vol. 45, pp. 713–22.
35. P. Gong, E.J. Palmiere, and W.M. Rainforth: *Acta Mater.*, 2015, vol. 97, pp. 392–403.
36. M. Maalekian, R. Radis, M. Militzer, A. Moreau, and W.J. Poole: *Acta Mater.*, 2012, vol. 60, pp. 1015–26.
37. C. Fossaert, G. Rees, T. Maurickx, and H.K.D.H. Bhadeshia: *Metall. Mater. Trans. A*, 1995, vol. 26A, pp. 21–30.
38. S.V. Subramanian, X. Ma, K. Rehman: *Proc. Energy Mater., Xi'an China*, 2014.
39. M.T. Nagata, J.G. Speer, and D.K. Matlock: *Metall. Mater. Trans. A*, 2002, vol. 33A, pp. 3099–3110.
40. B. Dutta, E.J. Palmiere, and C.M. Sellars: *Acta Mater.*, 2001, vol. 49, pp. 785–94.
41. F. Perrard, A. Deschamps, and P. Maugis: *Acta Mater.*, 2007, vol. 55, pp. 1255–66.
42. F. Perrard, A. Deschamps, F. Bley, P. Donnadieu, and P. Maugis: *J. Appl. Crystallogr.*, 2006, vol. 39, pp. 473–82.
43. K.Y. Xie, T. Zheng, J.M. Cairney, H. Kaul, J.G. Williams, F.J. Barbaro, C.R. Killmore, and S.P. Ringer: *Scr. Mater.*, 2012, vol. 66, pp. 710–13.
44. T. Gladman: *Mater. Sci. Technol.*, 1999, vol. 15, pp. 30–36.
45. M.F. Ashby:On the Orowan stress in *Physics of Strength and Plasticity*, A.S. Argon, ed., MIT Press, Cambridge, 1969, pp. 113–31.
46. A.J. Breen, K.Y. Xie, M.P. Moody, B. Gault, H.W. Yen, C.C. Wong, J.M. Cairney, and S.P. Ringer: *Microsc. Microanal.*, 2014, vol. 20, pp. 1100–10.
47. S.L. Shrestha, K.Y. Xie, C. Zhu, S.P. Ringer, C. Killmore, K. Carpenter, H. Kaul, J.G. Williams, and J.M. Cairney: *Mater. Sci. Eng. A*, 2013, vol. 568, pp. 88–95.
48. S.L. Shrestha, K.Y. Xie, S.P. Ringer, K.R. Carpenter, D.R. Smith, C.R. Killmore, and J.M. Cairney: *Scr. Mater.*, 2013, vol. 69, pp. 481–84.
49. A.G. Kostryzhev, A. Al Shahrani, C. Zhu, J.M. Cairney, S.P. Ringer, C.R. Killmore, and E.V. Pereloma: *Mater. Sci. Eng. A*, 2014, vol. 607, pp. 226–35.
50. A.J. Ardell: *Metall. Trans. A*, 1985, vol. 16A, pp. 2131–65.
51. E.V. Pereloma, A. Shekhter, M.K. Miller, and S.P. Ringer: *Acta Mater.*, 2004, vol. 52, pp. 5589–5602.
52. E.V. Pereloma, R.A. Stohr, M.K. Miller, and S.P. Ringer: *Metall. Mater. Trans. A*, 2009, vol. 40A, pp. 3069–75.
53. S.P. Ringer: *Mater. Sci. Forum*, 2006, vols. 519–521, pp. 25–34.